Chapter

Synthesis of Nanowire Using Glancing Angle Deposition and Their Applications

Chinnamuthu Paulsamy, Pheiroijam Pooja and Heigrujam Manas Singh

Abstract

Nanowires are highly attractive for advanced nanoelectronics and nanoscience applications, due to its novel properties such as increased surface area, large aspect ratio, and increased surface scattering of electrons and phonons. The design and fabrication of nanowires array provide a great platform to overcome the challenges/limitation of its counter partner. This chapter focuses on the synthesis of metal oxide nanowire and axial heterostructure nanowire array using the Glancing angle deposition (GLAD) technique. The structural, optical and electrical properties are studied. This GLAD technique offers control over one-dimensional (1D) nanostructure growth with self-alignment capability. It is also reviewed in an effort to cover the various application in this area of optoelectronic devices and wettability applications that had been synthesized using GLAD.

Keywords: nanowire, GLAD, heterojunction, photodetectors, wettability

1. Introduction

Low-dimensional nanostructures such as zero-dimensional (0D), one-dimensional (1D) and two-dimensional (2D) have attracted enormous attention from three-dimensional or bulk structure due to the novel physical and chemical properties caused by size and quantum effects. **Figure 1** illustrates the schematic representation of electron system in bulk structure and low-dimensional nanostructures. Quantum dot are 0D nanostructures with three quantum-confined directions. Quantum plane are 2D nanostructures with one quantum-confined direction, while two unconfined directions is available for movement of particle. Bulk structures are 0D structure with no quantum-confined directions. Nanowires (NWs) are 1D nanostructures with a large aspect ratio (length/diameter), with diameters in the 1–200 nm scale and lengths ranging from some hundreds of nanometers up to several tens of micrometer. Owing to their nanoscale dimensions, they have size confinement effects, which give them novel properties as compared to the bulk materials. Nanowires have two quantum-confined directions but one unconfined direction which is available for electrical conduction. The 1D geometry on the nanoscale of the nanowires provides an increased surface area, very high density of states, diameter dependent bandgap, and increased surface scattering of electrons and phonons [1]. These anisotropic properties are advantageous in nanoelectronics,

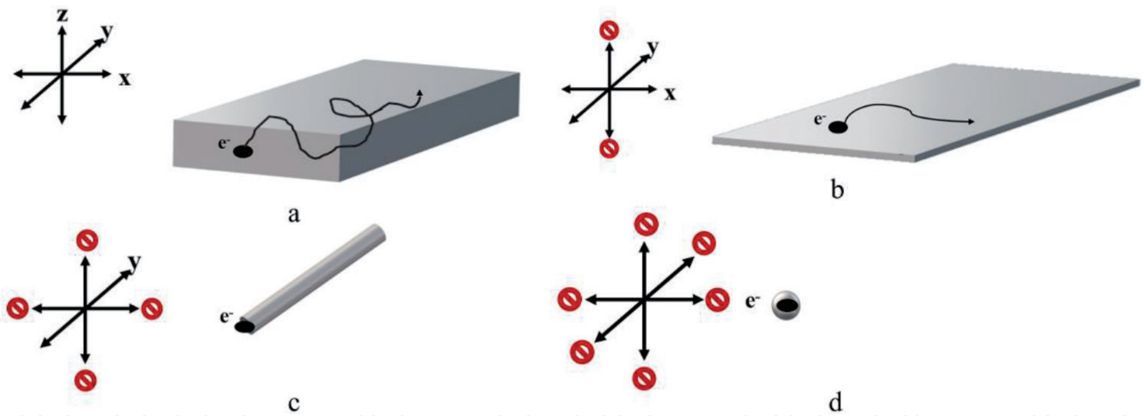

Figure 1.
Schematic illustration of electron system in (a) bulk structure, (b) quantum plane, (c) quantum wire, and (d) quantum dot.

photonics, optoelectronics, and bioengineering and have also generated great research interest [1, 2]. The concept of many advanced nanowire-based optoelectronics devices, including photodetectors, photovoltaic cells, has also been demonstrated, making nanowires promising material for advanced optoelectronics. Thus, nanowires draw considerable attention from those trying to apply nanotechnology as well as investigating in nanoscience.

Nanowires are the result of anisotropic, 1D growth on a nanometer scale. Therefore, the critical issue related to the growth of the nanowires is how to synthesize in a controlled manner. Regarding many approached have been employed, including the use of the nanolithography-based method [3], solution-based method [4], vapor-based methods [5], template-based methods [6], and glancing angle deposition (GLAD) technique [7]. Among these, the GLAD is a physical vapor deposition technique, which is a combination of oblique angle deposition and substrate positional control, which is most attractive owing to its simplicity and synthesis of different nanostructures with controlled porosity and shapes [7].

This chapter reviews the synthesis of nanowires by the GLAD technique and their applications. Furthermore, this chapter focuses on the GLAD technique. This chapter seeks to explain the understanding of the GLAD technique in the synthesis of nanowires. Accordingly, the chapter first reviews the fundamentals of the GLAD technique and the synthesis of nanowires. They are followed by some examples of optoelectronic devices and wettability applications of NWs that have been synthesized based on the GLAD technique.

2. Oblique angle deposition (OAD)

The glancing angle deposition (GLAD) technique is developed by Robbie and Brett [8], which is an extension to oblique angle deposition (OAD), where the substrate position is manipulated during the deposition. This section reviews the oblique angle deposition.

In OAD, the collimated evaporated beam is incident on the substrate surface normal with an incident angle α, as shown in **Figure 2(a)**. The incident vapor flux is treated as vector denoted by F, as shown in **Figure 2(b)** with its two components, a vertical component, and a lateral component. The arrival of incident vapor flux is a random process. During the deposition process, the impinging atoms will form islands on the substrate surface at random. The initial deposited seed will act as shadowing centers, and the tallest islands will receive more atoms as compared to the shorter ones. This phenomenon is known as the shadowing effect. With this procedure, only the tallest deposited material will grow into columns and thus result in a nanocolumn thin film formation. The lateral component is responsible for the shadowing effect. This leads to the inclination of the tilting of the nanostructure towards the direction of the incoming vapor flux, and the tilt angle is given by the tangent rule, $\tan\beta = \frac{1}{2}\tan\theta$. **Figure 3** shows how this effect takes place. In general, the columnar tilt angle β is less than the vapor flux incident angle [7].

The thin films deposited by OAD shows the following properties: Porous thin films acquiring nano-columnar structures. The nanocolumns tilt away from the substrate surface normal and towards the incident vapor flux direction.

2.1 Glancing angle deposition

The GLAD technique is developed based on the OAD with the only addition, which is the manipulation of the substrate position by using two stepper motors, one controls the incident angle, α, and the other motor controls the azimuthal rotation of the substrate with respect to the substrate surface normal. **Figure 4** shows the GLAD setup. The tilting of the nanocolumn structure found in OAD is mitigated primarily to the rotation of the substrate, which cancels out the lateral component of the incident vapor flux during the deposition process. By changing the speed and phase of the azimuthal rotation along with the deposition rate, different sculptures of nanocolumns such as C-shape, S-shape, helical or vertical nanocolumns can be achieved.

The nanocolumns synthesized by GLAD show the following properties: The porosity of the film is controlled by changing the incident angle. Self-alignment is

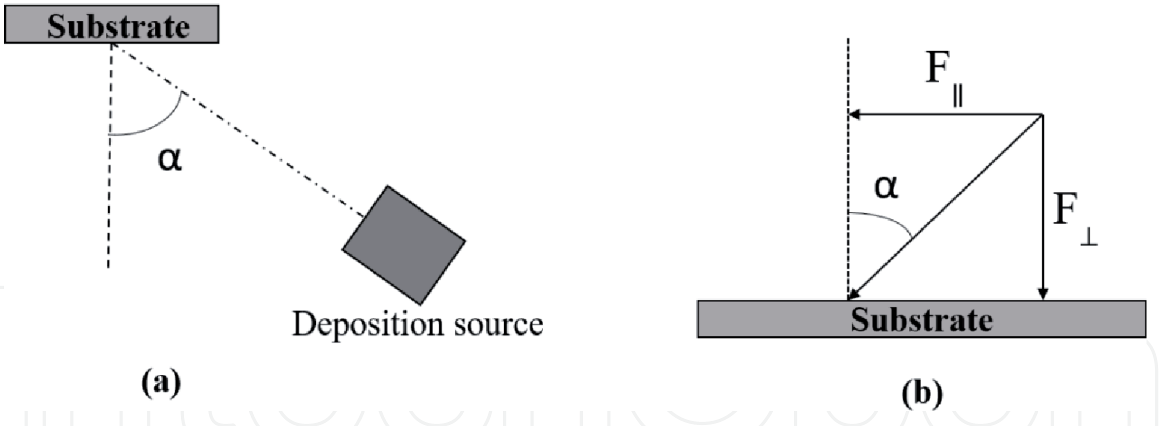

Figure 2.
(a) Experimental setup for OAD and (b) incident vapor flux components.

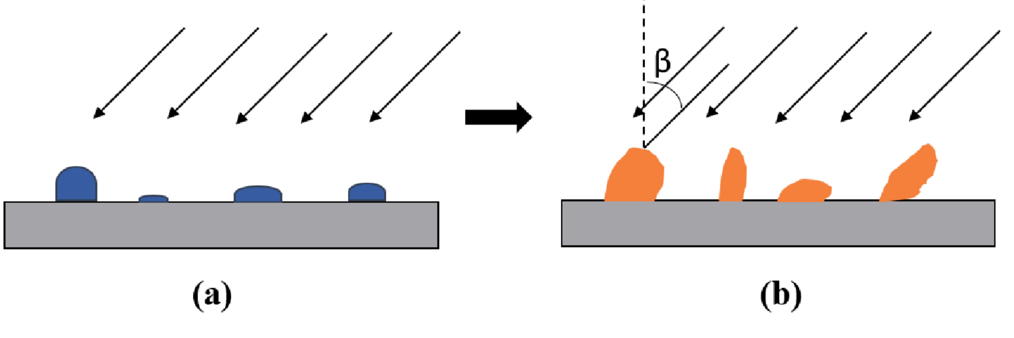

Figure 3.
The shadowing effect during OAD (a) initial nucleation to form shadowing centres, and (b) columnar structures formed due to the shadowing effect.

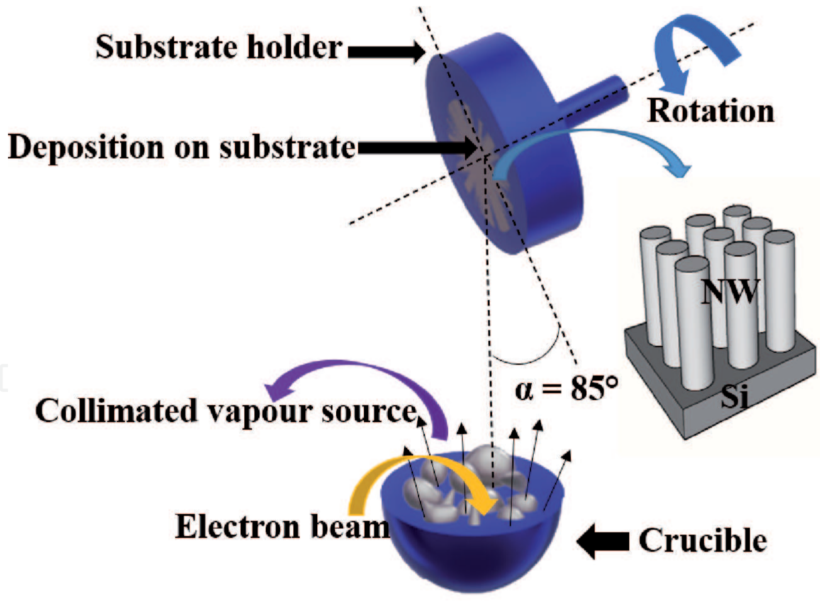

Figure 4.
Experimental setup for GLAD.

due to the shadowing effect. The shape and in-plane alignment of nanocolumns can be modified. GLAD is compatible with a large number of materials [9]. **Table 1** summarizes the synthesis of nanowires using the GLAD technique. The following sections give examples of the various applications of nanowires synthesized using the GLAD technique. The general experimental conditions are the following: the experiments were performed in an electron-beam evaporator (BC 300 HHV India) incorporated with GLAD under high vacuum pressure (6×10^{-6} mbar) inside the chamber. The deposition rate varied from 0.5–1 Å/s, and rotation speed was maintained at 20–30 rpm. The substrate holder was oriented at 85° with respect to the source. During the deposition process, the growth rate was monitored by using a quartz crystal-based digital thickness monitor inside the chamber.

2.2 Properties of nanowires synthesized using GLAD

This section discusses the structural and optical properties of nanowires. For various applications, characterizing the structural, optical, and electrical properties of nanowires is important so that the interrelationship can be investigated and established. Nanowires synthesized using the same material under the same experimental conditions may possess different properties due to the differences in structural properties.

2.2.1 Structural characterization

Structural properties of a nanowire help in determining the various attribute like optical and electrical properties. X-ray diffraction (XRD), scanning electron microscope (SEM), transmission electron microscope (TEM) are used to investigate the structural properties of nanowires. XRD characterization provides crystal structure information. The peak in XRD provides the crystal phase structure long with growth direction. SEM produces images of the nanowires down to the length scale of ~100 nm, which gives information regarding the structural arrangement, geometrical features of the nanowire. For example, SEM images of TiO_2 nanowire arrays grown on Si substrate provide evidence for shadowing effect as well as

Material	Deposition method	Reference
TiO_2	Electron beam	[10–15]
TiO_2/In_2O_3	Electron beam	[16]
SnO_2	Electron beam	[17]
WO_2	Electron beam	[18]
Er_2O_3-doped SnO_2	Electron beam	[19]
Er_2O_3	Electron beam	[20]
Er-doped TiO_2	Electron beam	[21, 22]
Co_3O_4-TiO_2	Electron beam	[23]
SiO_x-In_{2-x} O_{3-y}	Electron beam	[24]
Ge	Electron beam	[25]

Table 1.
Summary of nanowires synthesized using the GLAD technique.

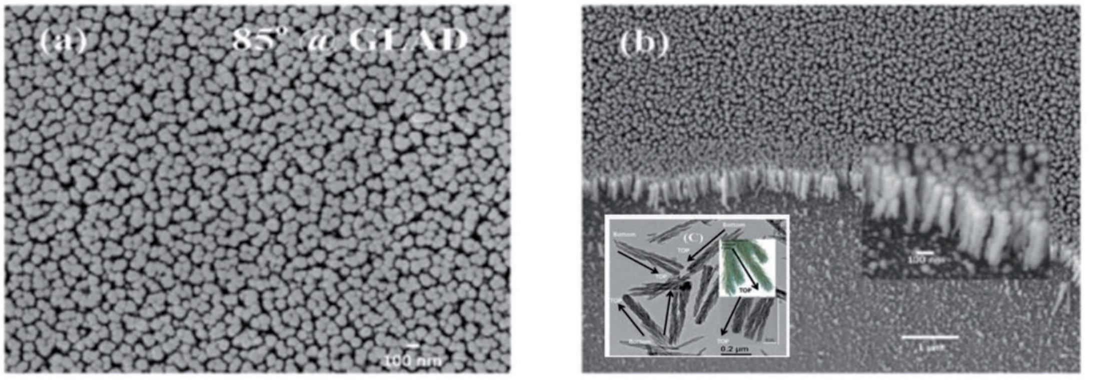

Figure 5.
FE-SEM and HR-TEM images of TiO2 nanowire: (a) top view, (b) side view, and (c) HR-TEM images (inset). Adapted from Ref. [15].

information on the geometry of the nanowires, as shown in **Figure 5(a)** and **(b)**. TEM is used for studying the nanowire at the atomic scale. Furthermore, selected area electron diffraction (SAED) patterns provide information on the crystal structure of nanowires. For example, TEM image of TiO_2 provide information on the geometry of the nanowires at nanoscale along with growth direction as shown in inset **Figure 5(c)**.

2.2.2 Optical characterization

The optical characterization of nanowires provides information on properties different from those of the bulk forms. Optical measurements like absorption and photoluminescence provide information on the absorption and emission of light in frequency range varying from UV-Vis-NIR spectra. Absorption measurement aids in determining the bandgap of the grown nanowire shown in **Figure 6**. The difference in the optical properties is due to the geometric differences such as the diameter and length of nanowires.

Photoluminescence (PL) measurement studies the optical bandgap, oxygen vacancies, and defect states in nanowires. For example, **Figure 7** investigates the PL spectrum of TiO_2 NW under 250 nm wavelength excitation.

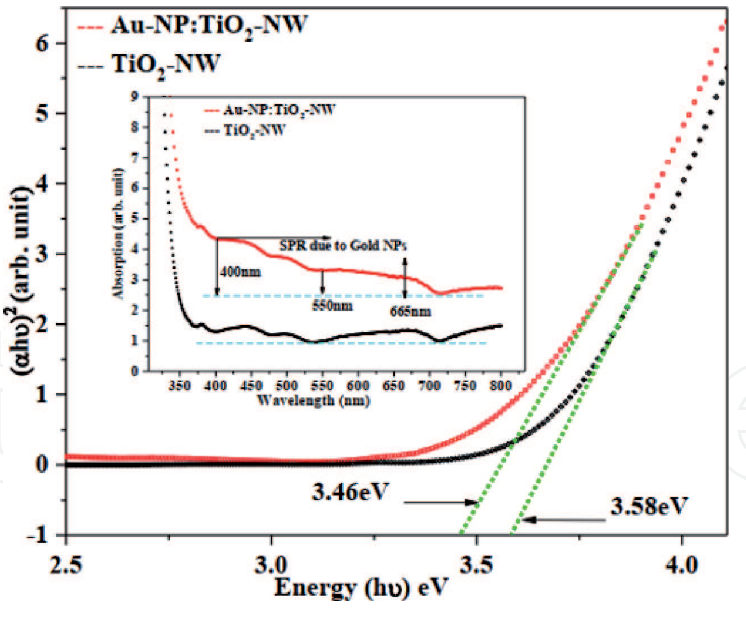

Figure 6.
Tauc plot of Au-NP:TiO_2-NW and TiO_2-NW, inset: UV-Vis absorption of both samples. Adapted from Ref. [10].

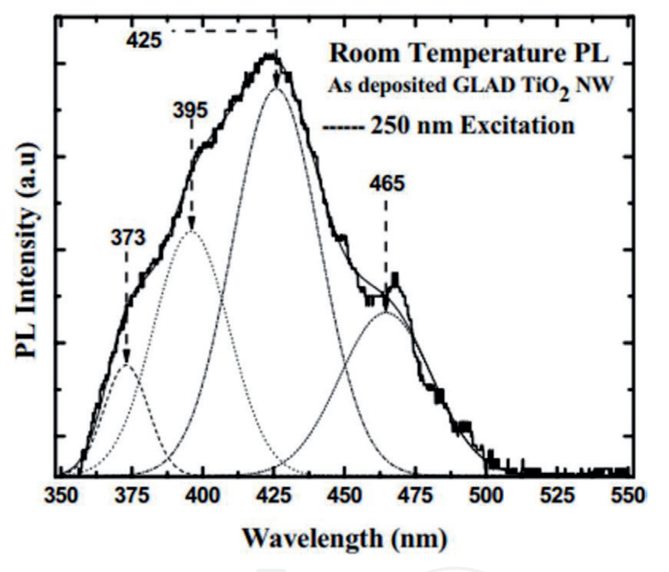

Figure 7.
Room temperature PL spectrum of as deposited TiO_2 nanowire. Adapted from Ref. [15].

3. Applications

In the preceding sections, we have discussed the central characteristics of nanowires, which attracts attention to find the application by using its novel properties compared to their bulk materials. Based on the GLAD technique, many conceptual devices have already been reported. In this section, selected applications of GLAD synthesized nanowires such as photodetectors and wettability applications are discussed. These conceptual devices were investigated based on an array of nanowires. First, the silicon (Si) substrate is subjected to a 3-step cleaning process using electronic grade acetone, methanol, and deionized (DI) water, and then an array of nanowires is synthesized on the Si substrate. The top metal contact electrode is synthesized on the nanowire arrays through an Al mask with a hole diameter ~1 mm and ITO, which is used as the back-contact electrode.

3.1 Photodetector

Semiconductor photodetectors are devices used for the detection of light. More specifically, photodetectors have applications in optical communication, flame detection, chemical, and biological detection [26]. The PN junction is one of the most commonly used configurations for semiconductor photodetectors. Many researchers have synthesized nanowire and axial heterostructure nanowire array-based photodetectors using GLAD technique. **Table 2** gives a summary of the figure of merit for the photodetectors. These photodetectors are used for the detection of UV and visible light. The performance of photodetector is evaluated by investigation of various parameters such as photosensitivity, responsivity, detectivity, and noise equivalent ratio. The photosensitivity for photodetectors is calculated from the ratio of light current to dark current given by equation below:

$$\text{Photsensitivity} = \frac{I_{\text{Photo}} - I_{\text{Dark}}}{I_{\text{Dark}}} \tag{1}$$

The responsivity at a particular wavelength is computed from the ratio of photocurrent to incident optical power defined below:

$$R_{\lambda} = \frac{I_{\text{Photo}}}{P_{\text{Opto}}} \tag{2}$$

where I_{Photo} is the photocurrent and P_{opto} is the optical power. The detectivity and NEP give the noise performance of photodetectors. Detectivity is given by

$$D^{*} = \frac{R_{\lambda}}{\sqrt{2eJ_{\text{Dark}}}} \tag{3}$$

where J_{Dark} is the dark current density, e is the charge of electron and R_{λ} is the responsivity at a particular wavelength. The NEP is expressed as

$$\text{NEP} = \frac{\sqrt{A}\sqrt{B}}{D^{*}} \tag{4}$$

where A is the area of device and B is the bandwidth. The bandwidth is assumed to be 1 kHz as the flicker noise. With these relations, detectivity and NEP are plotted as a function of voltage to evaluate the performance of photodetector. Furthermore, the photocurrent-time response gives the temporal response under light on-off to study the switching behavior at a fixed voltage. The cumulative analysis of the figure of merit for photodetectors supports that the synthesis of nanowire and axial heterostructure nanowire array-based photodetectors using the GLAD technique as a potential prospect to fulfill the requirements of commercial UV-Visible photodetectors.

Device structure	Wavelength (nm) (voltage bias)	Responsivity	Detectivity (Jones)	NEP	Rise time	Fall time	Ref.
TiO_2-NW/p-Si	370 (−7 V)	28.38 A/W	4.97×10^{11}	5.6×10^{-12} W	0.30 s	0.18 s	[10]
Au-NP:TiO_2-NW/p-Si	370 (−7 V)	43.27 A/W	2.63×10^{12}	1.0×10^{-12} W	0.15 s	0.17 s	[10]
TiO_2/In_2O_3 AH NW	380 (−4.5 V)	11.17 A/W	3.14×10^{14}	8.9×10^{-15} W	52.96 ms	89.32 ms	[16]
WO_3	360 (3 V)	9.66 A/W	5.94×10^{12}	—	1.78 s	1.09 s	[18]
		50.95 A/W (annealed)	1.05×10^{13}	—	1.33 s	0.94 s	
Ag/Er_2O_3/Si	210 (−3 V)	0.527 A/W	$1{:}18 \times 10^{12}$	2.37 pW	0.28 s	0.18 s	[20]

Table 2.
Summary of the figure of merit for photodetectors.

3.2 Wettability application

In today's world, various technologies have been obtained from nature. Among them, self-cleaning technology is one of it. Many surfaces found in nature show self-cleaning properties. The leaves of plants such as lotus [27] and wings of butterflies [28] are a few examples. Self-cleaning technology obtained a lot of attention in the late 20th century for applications ranging from solar panel cleaning, windowpane cleaning, and textiles to cement. In recent years, many research works are carried out to develop durable and efficient self-cleaning coating surfaces with improved optical qualities. The self-cleaning coating can be classified into two categories: hydrophobic and hydrophilic coatings. In the hydrophobic coating technique, water droplets roll and slide over the surfaces and clean them, while in the hydrophilic technique, water forms a sheet of water over the surfaces and carries the dirt and other impurities away. The phenomenon of self-cleaning is associated with surface contact angle, which is the angle formed between the surfaces of the liquid droplet to the solid surface. Generally, when the contact angle is less than 90^0, the solid surface is defined as a hydrophilic surface (**Figure 8(a)**). If the contact angle is greater than 90^0, the surface is termed as a hydrophobic surface (**Figure 8(b)**). Likewise, the surface with a water contact angle close to zero is defined as super hydrophilic, and surface with a contact angle greater than 150^0 is categorized as super hydrophobic (**Figure 8(c)**).

Young in 1805 proposed a model to define the state of liquid droplet on an ideal rigid surface [29]. The equation defined by Young's model is given as:

$$\gamma_{SG} = \gamma_{SL} + \gamma_{LG} \cos\theta_Y \tag{5}$$

θ_Y is the water contact angle and Υ_{SG}, Υ_{SL} and Υ_{LG} are the interfacial surface tensions of solid and gas, solid and liquid, liquid and gas, respectively. This

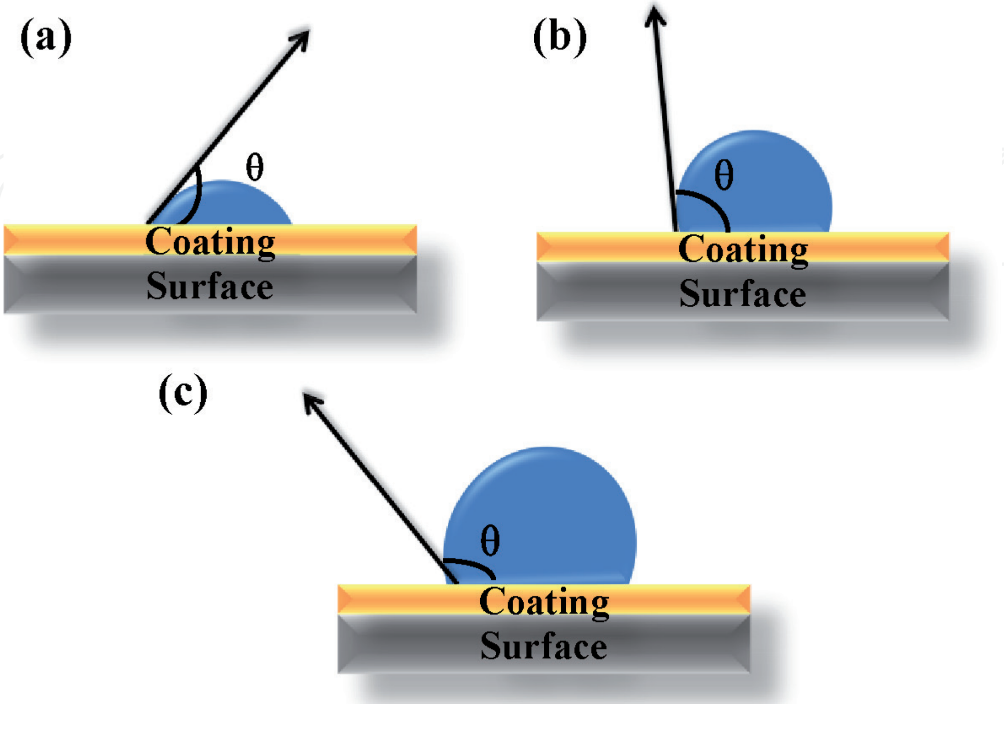

Figure 8.
Schematic diagram of (a) hydrophilic (θ < 90°), (b) hydrophobic (θ > 90°), and (c) super hydrophobic (θ > 150°) surfaces.

equation shows the water contact angle of a liquid droplet on solid surface from the three surface tensions. As seen in **Figure 9(a)**, an equilibrium state is reached between these three surface tensions, and the contact angle is given by the angle between Υ_{SL} and Υ_{LG}. In 1936, Wenzel further purposed a model to describe homogeneous wetting regimes [30]. This wetting regime for water contact angle on rough surfaces is defined by the equation given below:

$$\cos\theta_W = r\cos\theta_Y \tag{6}$$

where θ_W and θ_Y represent apparent contact angle and Young's contact angle for an ideal rigid surface respectively while r represents the surface roughness factor, which is the ratio of true solid surface area to the apparent surface area. This model states on the affiliation between the structure and surface tension of a homogeneous surface. In **Figure 9(b)**, the true surface area is larger than the apparent surface area, thus the value of r is greater than 1. Wenzel's model is applicable to surface with single chemical component and thermodynamically stable state, which limits its applications in heterogeneous surfaces. In 1944, Cassie and Baxter defined an equation to describe contact angle for composite surfaces [31].

$$\cos\theta_C = f_1\cos\theta_1 + f_2\cos\theta_2, \left(f_1 + f_2 = 1\right) \tag{7}$$

Where θ_C is apparent contact angle in Cassie–Baxter model, θ_1 and θ_2 are intrinsic contact angle of first and second components, respectively. f_1 and f_2 are apparent area fraction of first and second component, respectively. In general, if either one of surface component is air, then $\theta_2 = 180^0$.

$$\cos\theta_C = f_1\cos\theta_1 - f_2 = f_1\left(\cos\theta_1 + 1\right) - 1 \tag{8}$$

Figure 9(c) displays a water droplet on surface showing hydrophobic property due to surface composed of air and hydrophobic component.

Metal oxides such as TiO_2, SnO_2, and ZnO have been used as a self-cleaning and antifogging surface [32, 33]. Metal oxides are known to have good stability and transparency, which enable tuning wettability on application of proper radiation. Amidst them, TiO_2 is vastly studied due to its effective photocatalytic activity as it washes off dirt or decomposes organic contaminants from surfaces [34]. Moreover, TiO_2 is known for its nontoxicity, chemical, and thermal stability [16, 35, 36]. Moreover, growth of perpendicularly aligned coaxial TiO_2/In_2O_3 NW on Si substrate is problematic due to limited growth techniques. Here, coaxial TiO_2/In_2O_3 NW assembly deposited employing GLAD technique inside electron beam evaporator [37] showed comparatively faster photo-induced wettability tuning within 10 min illumination than the reported SnO_2 doped with Fe thin film deposited using spin coating [38], TiO_2 films deposited using metal-organic chemical vapor deposition process [39], grapheme films prepared using chemical vapor deposition (CVD) method [40], TiO_2 films were fabricated on stainless steel substrates via electrophoretic deposition (EPD) [41]. Based on Cassie-Baxter relation, the water contact angle of TiO_2/In_2O_3 NW was found to be 129°. **Figure 10(a)** shows coaxial TiO_2/In_2O_3 NW FESEM side view and inset of **Figure 3(b)** schematic of TiO_2/In_2O_3 NW. In 1D NW heterostructure, there is more surface area to volume ratio and allows charge carriers to flow with less scattering enabling more carriers interaction with water as compared with uniform thin films. Vertically aligned NWs also acquires

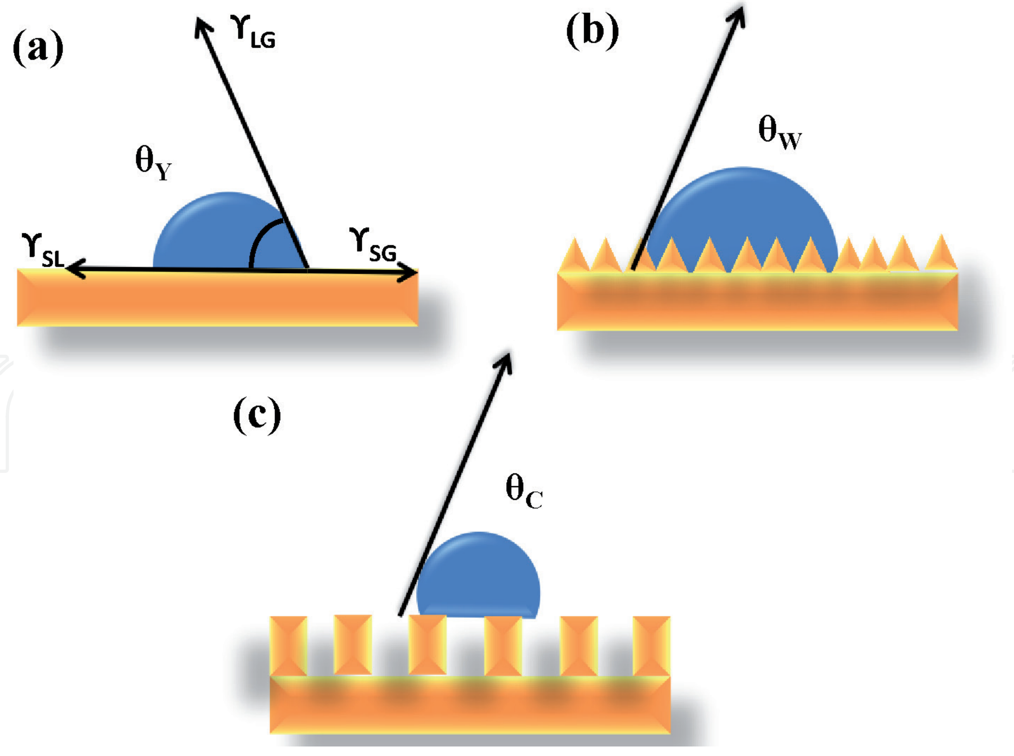

Figure 9.
(a) A liquid droplet on smooth surface in young model, (b) a liquid droplet on rough surface in Wenzel model, and (c) a liquid droplet on rough and porous surface in Cassie and Baxter model.

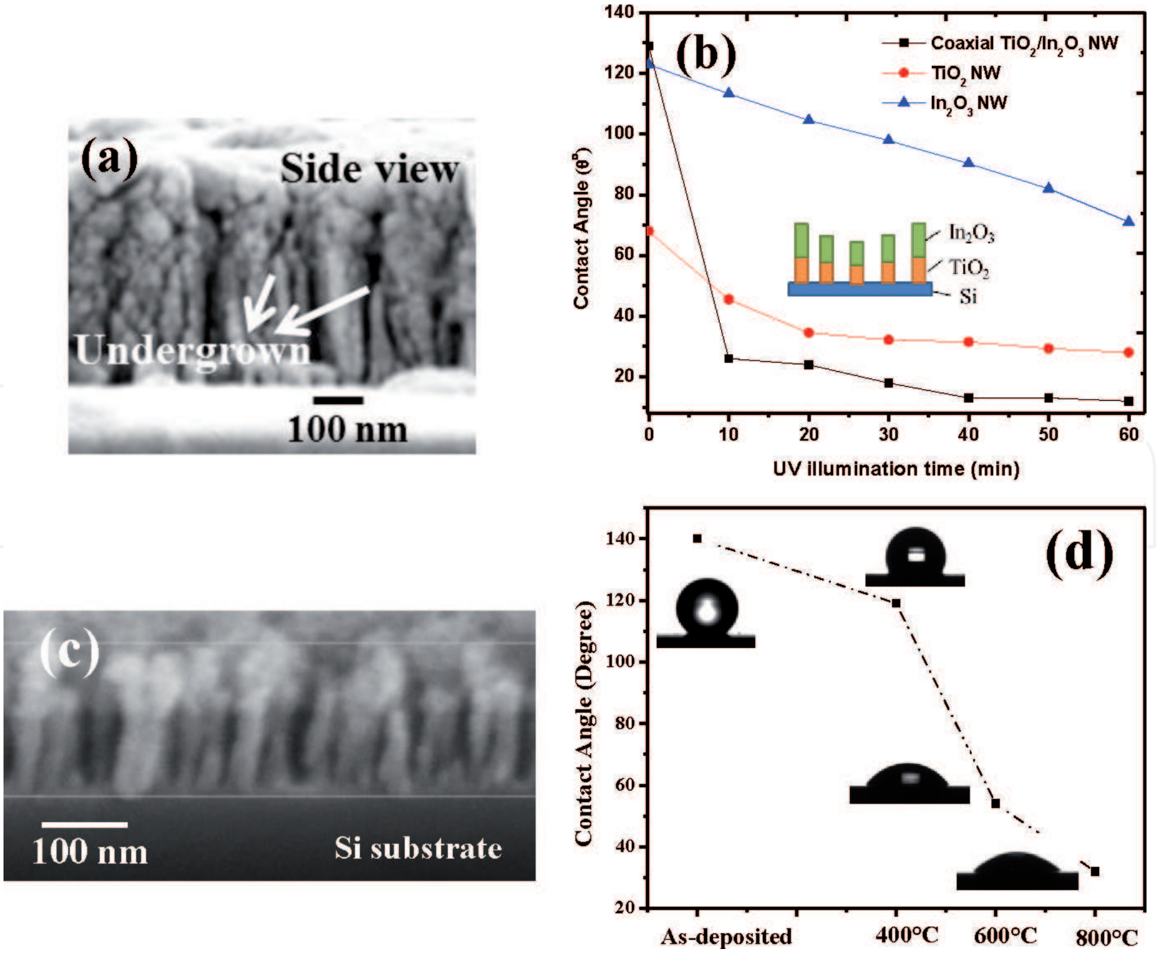

Figure 10.
(a) Coaxial TiO_2/In_2O_3 NW FESEM side view, (b) water contact angle variation under UV illumination of coaxial TiO_2/In_2O_3 NW, TiO_2 NW and In_2O_3 NW (inset schematic of TiO_2/In_2O_3 NW), (c) 600°C annealed TiO_2/In_2O_3 NW FESEM side view, and (d) static contact angle of as-deposited TiO_2-In_2O_3 NWs and annealed samples. Adapted from Ref. [37, 42].

characteristics such as low reflectivity and multiple scattering of light, which increase the carriers generation and thus more interaction of separated photogenerated charge carriers with water molecules to adsorb on the surface comparing with thin film. Moreover, TiO_2/In_2O_3 NW (1.2×10^{-3} degree^{-1} min^{-1}) showed better wettability transition rate than TiO_2 NW (3.2×10^{-4} degree^{-1} min^{-1}) and In_2O_3 NW (9.2×10^{-5} degree^{-1} min^{-1}) due to the interfacial surface modification between TiO_2 and In_2O_3 and effective interaction between photogenerated charge carriers with water molecules (**Figure 10(b)**) [37]. All these assure prospective applications of coaxial TiO_2/In_2O_3 NW grown using the GLAD technique for smart surfaces, with controlled switchable wettability by external stimuli for self-cleaning applications.

Further, TiO_2/In_2O_3 NW surface wettability had been tuned by annealing treatment, without changing the surface with extra chemical coating or by external light stimuli [42]. **Figure 10(c)** shows 600°C Annealed TiO_2/In_2O_3 NW FESEM side view. TiO_2/In_2O_3 NW samples annealed at 600°C shows nearly superhydrophilic with static water contact angle of 12° (**Figure 10(d)**). The surface of TiO_2/In_2O_3 NW had been controlled to acquire desired water contact angles, which is paramount for designing practical application in self-cleaning, electronic, and biomedical fields.

4. Conclusion

In this capture, we have reviewed the synthesis of nanowires using GLAD and their applications. We have showed that GLAD is a simple, cost effective, and catalytic free technique where well-defined vertically aligned nanostructures can be synthesized which cannot be achieved easily by nanolithography-based method, solution-based method, vapor-based methods, template-based methods. Nanowires synthesized by GLAD technique has the following advantages: Growth of vertically aligned nanostructure, the shadowing effect introduces self-alignment effect, the porosity of the nanostructure film can be controlled by changing the incident angle. Various applications of nanowire and axial heterostructure nanowire array-based photodetectors as well as wettability applications synthesized using the GLAD technique have been discussed. The performance of these applications can be improved further with different structural and growth parameters. Therefore, it can be concluded that these nanoscale-based applications have potential for future industrial and commercial applications.

Acknowledgements

The authors are grateful and would like to acknowledge, NIT Nagaland and TEQIP-III for providing the synthesis and characterization facility.

Conflict of interest

The authors declare no conflict of interest.

Author details

Chinnamuthu Paulsamy*, Pheiroijam Pooja and Heigrujam Manas Singh
Department of Electronics and Communication Engineering, NIT Nagaland, India

*Address all correspondence to: chinnamuthu@nitnagaland.ac.in

References

[1] Dresselhaus MS, Lin Y-M, Rabin O, Black MR, Kong J, Dresselhaus G. Nanowires. In: Bhushan B., editor. Springer Handbook of Nanotechnology,. Springer Handbooks. Springer; 2010. p. 119-167. DOI: 10.1007/978-3-642-02525-9_4

[2] Z. Pei L, Y. Cai Z. A Review on Germanium Nanowires. Recent Pat Nanotechnol 2011;6:44-59. DOI: 10.2174/187221012798109291

[3] Chen Y, Pepin A. Nanofabrication: Conventional and nonconventional methods. Electrophoresis 2001;22:187-207. DOI: 10.1002/1522-2683(200101)22:2%3C187::AID-ELPS187%3E3.0.CO;2-0

[4] Trentler TJ, Hickman KM, Goel SC, Viano AM, Gibbons PC, Buhro WE. Solution-liquid-solid growth of crystalline III-V semiconductors: An analogy to vapor-liquid-solid growth. Science 1995;270:1791-4. DOI: 10.1126/science.270.5243.1791

[5] Yang P, Wu Y, Fan R. Inorganic semiconductor nanowires. Int J Nanosci 2002;1:1-39. DOI: 10.1142/S0219581X02000061

[6] Hulteen J. A general template-based method for the preparation of nanomaterials. J Mater Chem 1997;7:1075-87. DOI: 10.1039/A700027H

[7] Zhao Y, Ye D, Wang G-C, Lu T-M. Designing nanostructures by glancing angle deposition. Proc.SPIE 5219. Nanotube and Nanowires 2003. DOI: 10.1117/12.505253

[8] Zhou CM, Gall D. Growth competition during glancing angle deposition of nanorod honeycomb arrays. Appl Phys Lett 2007;90:1-4. DOI: 10.1063/1.2709929

[9] Taschuk MT, Hawkeye MM, Brett MJ. Glancing Angle Deposition. Third Edit. Elsevier Ltd.; 2010. https://doi.org/10.1016/B978-0-8155-2031-3.00013-2.

[10] Kashyap KK, Choudhuri B, Chinnamuthu P. Enhanced Optical and Electrical Properties of Metallic Surface Plasmon Sensitized TiO_2 Nanowires. IEEE Trans Nanotechnol 2020;19:519-26. DOI: 10.1109/TNANO.2020.3004876

[11] Ngangbam C, Singh NK, Mondal A. Effect of Ag Doping on the Glancing Angle Deposition Synthesized TiO_2 Nanowire for Enlarged Photodetection . J Nanosci Nanotechnol 2017;18:5059-62. DOI: 10.1166/jnn.2018.15337

[12] Chinnamuthu P, Mondal A, Dhar JC, Singh NK. Visible light detection using glancing angle deposited TiO_2 nanowire arrays. Jpn J Appl Phys 2015;54:4-7. DOI: 10.7567/JJAP.54.06FJ01

[13] Dhar JC, Mondal A, Singh NK, Chinnamuthu P. Low-leakage TiO_2 nanowire dielectric MOS device using Ag schottky gate contact. IEEE Trans Nanotechnol 2013;12:948-50. DOI: 10.1109/TNANO.2013.2277600

[14] Mondal A, Dhar JC, Chinnamuthu P, Singh NK, Chattopadhyay KK, Das SK, et al. Electrical properties of vertically oriented TiO_2 nanowire arrays synthesized by glancing angle deposition technique. Electron Mater Lett 2013;9:213-7. DOI: 10.1007/s13391-012-2136-5

[15] Chinnamuthu P, Dhar JC, Mondal A, Bhattacharyya A, Singh NK. Ultraviolet detection using TiO_2 nanowire array with Ag Schottky contact. J Phys D Appl Phys 2012;45. DOI: 10.1088/0022-3727/45/13/135102

[16] Pooja P, Chinnamuthu P. Surface state controlled superior photodetection properties of isotype n-TiO_2/In_2O_3 heterostructure nanowire array with

high specific detectivity. IEEE Trans Nanotechnol 2020;19:34-41. DOI: 10.1109/TNANO.2019.2956960

[17] Chetri P, Dhar JC. Improved photodetector performance of SnO_2 nanowire by optimized air annealing. Semicond Sci Technol 2020;35:45014. DOI: 10.1088/1361-6641/ab7434

[18] Rajkumari R, Singh NK. Effect of Annealing on the Structural and Electrical Properties of GLAD Synthesized Vertical Aligned WO_3 Nanowire. IEEE Trans Nanotechnol 2019;18:676-83. DOI: 10.1109/TNANO.2019.2927367

[19] Panigrahy S, Dhar JC. Non-volatile memory property of Er_2O_3 doped SnO_2 nanowires synthesized using GLAD technique. J Mater Sci Mater Electron 2019;0:0. DOI: 10.1007/s10854-019-01151-0

[20] Panigrahy S, Dhar JC. Post Annealing Effects on Er_2O_3 Nanowire Arrays for Improved Photodetection. IEEE Trans Nanotechnol 2018;17:1189-96. DOI: 10.1109/TNANO.2018.2869223

[21] Lahiri R, Ghosh A, Choudhuri B, Mondal A. Investigation on improved performance of Erbium doped TiO_2 nanowire based UV detector. Mater Res Bull 2018;103:259-67. DOI: 10.1016/j.materresbull.2018.03.024

[22] Lahiri R, Mondal *A. superior* memory of Er-doped TiO_2 nanowire MOS capacitor. IEEE Electron Device Lett 2018;39:1856-9. DOI: 10.1109/LED.2018.2874272

[23] Choudhuri B, Mondal A, Dwivedi SMMD, Henini M. Fabrication of novel transparent Co_3O_4-TiO_2 nanowires p-n heterojunction diodes for multiband photodetection applications. J Alloys Compd 2017;712:7-14. DOI: 10.1016/j.jallcom.2017.04.068

[24] Singh NK, Mondal A, Dhar JC, Chakrabartty S, Chattopadhyay KK, Bhattacharyya A. Improved photodetection from annealed SiO_x-$In_{2-x}O_{3-y}$ axial heterostructure nanocolumns. J Phys D Appl Phys 2014;47. DOI: 10.1088/0022-3727/47/10/105106

[25] Singh HM, Choudhuri B, Chinnamuthu P. Investigation of optoelectronic properties in germanium nanowire integrated silicon substrate using kelvin probe force microscopy. IEEE Trans Nanotechnol 2020;19;628-34. DOI: 10.1109/TNANO.2020.3010691

[26] Monroy E, Omnès F, Calle F. Wide-bandgap semiconductor ultraviolet photodetectors. Semicond Sci Technol 2003;18:R33. DOI: 10.1088/0268-1242/18/4/201

[27] Dorrer C, Rühe J. Some thoughts on superhydrophobic wetting. Soft Matter 2009;5:51-61. DOI: 10.1039/B811945G

[28] Byun D, Hong J, Ko JH, Lee YJ, Park HC, Byun B-K, et al. Wetting characteristics of insect wing surfaces. J Bionic Eng 2009;6:63-70. DOI: 10.1016/S1672-6529(08)60092-X

[29] Young T. III. An essay on the cohesion of fluids. Philos Trans R Soc London 1805:65-87. DOI: 10.1098/rstl.1805.0005

[30] Wenzel RN. Resistance of solid surfaces to wetting by water. Ind Eng Chem 1936;28:988-94. DOI: 10.1021/ie50320a024

[31] Cassie ABD, Baxter S. Wettability of porous surfaces. Trans Faraday Soc 1944;40:546-51. DOI: 10.1039/TF9444000546

[32] Miyauchi M, Nakajima A, Watanabe T, Hashimoto K. Photocatalysis and photoinduced hydrophilicity of various metal oxide thin films. Chem Mater 2002;14:2812-6. DOI: 10.1021/cm020076p

[33] Kenanakis G, Vernardou D, Katsarakis N. Light-induced self-cleaning properties of ZnO nanowires grown at low temperatures. Appl Catal A Gen 2012;411:7-14. DOI: 10.1016/j.apcata.2011.09.041

[34] Fujishima A, Zhang X, Tryk DA. TiO_2 photocatalysis and related surface phenomena. Surf Sci Rep 2008;63: 515-82. DOI: 10.1016/j.surfrep.2008.10.001

[35] Yasui M, Katagiri K, Yamanaka S, Inumaru K. Molecular selective photocatalytic decomposition of alkylanilines by crystalline TiO_2 particles and their nanocomposites with mesoporous silica. RSC Adv 2012;2:11132-7. DOI: 10.1039/C2RA21009F

[36] Xu C, Yuan Y, Yuan R, Fu X. Enhanced photocatalytic performances of TiO_2-graphene hybrids on nitro-aromatics reduction to amino-aromatics. RSC Adv 2013;3:18002-8. DOI: 10.1039/C3RA42579G

[37] Pooja P, Choudhuri B, Saranyan V, Chinnamuthu P. Synthesis of coaxial TiO_2/In_2O_3 nanowire assembly using glancing angle deposition for wettability application. Appl Nanosci 2019;9:529-37. DOI: 10.1007/s13204-018-0936-0

[38] Talinungsang, Purkayastha DD, Krishna MG. Dopant controlled photoinduced hydrophilicity and photocatalytic activity of SnO_2 thin films. Appl Surf Sci 2018;447:724-31. DOI: 10.1016/j.apsusc.2018.04.028

[39] Miyauchi M, Kieda N, Hishita S, Mitsuhashi T, Nakajima A, Watanabe T, et al. Reversible wettability control of TiO_2 surface by light irradiation. Surf Sci 2002;511:401-7. DOI: 10.1016/S0039-6028(02)01551-0

[40] Xu Z, Ao Z, Chu D, Younis A, Li CM, Li S. Reversible hydrophobic to hydrophilic transition in graphene via water splitting induced by UV irradiation. Sci Rep 2014;4:1-9. DOI: 10.1038/srep06450

[41] Toh AGG, Nolan MG, Cai R, Butler DL. Reversible wetting of titanium dioxide films. Device Process Technol. Microelectron. MEMS, Photonics, Nanotechnol. IV, vol. 6800, International Society for Optics and Photonics; 2008, p. 680004. DOI: 10.1117/12.759438

[42] Pooja P, Chinnamuthu P. Annealing Effect of Glancing Angle Electron Beam Deposited TiO_2/In_2O_3 Nanowires Array on Surface Wettability. Sci Rep 2020;10:1-8. DOI: 10.1038/s41598-020-66150-2